DOI: 10.1002/ejic.200701308

Synthesis and Characterisation of Some New Zinc Carbamate Complexes Formed by CO_2 Fixation and Their Use as Precursors for ZnO Particles under Mild Conditions

Dan Domide,[a] Elisabeth Kaifer,[a] Jürgen Mautz,[a] Olaf Walter,[b] Silke Behrens,[b] and Hans-Jörg Himmel*[a]

Keywords: CO_2 fixation / Zinc oxide / Precursor chemistry / Carbamate complexes

Herein we report on CO_2 fixation by insertion into the Zn–N bonds of the two molecular compounds $EtZnN(iPr)_2$ and $EtZnN(iBu)_2$. The tetrameric carbamate complexes $[EtZn(O_2CNR_2)]_4$ (R = *i*Pr and *i*Bu) were found to be the products of these reactions. The structures of the complexes were established by single-crystal X-ray diffraction. Thermal decomposition of the carbamate complexes was studied by applying a variety of different analytical techniques. These studies show that the compounds are suitable precursors for nanosized ZnO particles of ca. 10 nm diameter synthesised under mild conditions (< 200 °C) with the oxygen atoms originating from the reactant CO_2.

Introduction

From the possible routes to zinc carbamate complexes, which have been reported in the past, the following three involve direct reactions with CO_2: (i) electrochemical oxidation of anodic zinc in the presence of a nitrogen base and CO_2, (ii) autoclave reaction between Zn powder and a secondary amine at high temperatures and CO_2 pressures, and (iii) reactions of ZnX_2 (X = halogen or alkyl) with a secondary amine and CO_2. While Zn is oxidised in the first two routes from Zn^0 to Zn^{II}, the third route already starts with a Zn^{II} compound. An example for the first route (which is relatively uncommon) is provided by the formation of the carbamate complex **1** (see Scheme 1).[1] Interestingly, this example features a μ^1-coordinated carbamato ligand while the other examples shown here feature predominantly μ^2-coordinated carbamato ligands. The direct use of the liquid 1:1 adduct of $HNMe_2$ and CO_2, which can be formulated as a dimethylammonium carbamate salt $[NH_2Me_2][O_2CNMe_2]$[2] in the electrolysis in acetonitrile, leads to $[NH_2Me_2][Zn_2(O_2CNMe_2)_5]$ with three bridging and two terminal carbamato units.[3] An example for the second route is the autoclave reaction between zinc powder and $HNEt_2$ at 150 °C and 50 atm of CO_2 in toluene.[4] $[Zn_4O(O_2CNEt_2)_6]$ (**2**; Scheme 1) featuring a μ^4-coordinated O atom in the centre is the characterised product of this reaction. It has been claimed that the oxygen atom stems from deoxygenation of the CO_2 (the redox reaction thus comprising reduction of the C atoms and oxidation of Zn). Complexes of the formula $[Zn_4O(O_2CR)_6]$ (R = diethylamino, piperidino, and pyrrolidino) are also accessible using standard Schlenk techniques, e.g. by addition of H_2O

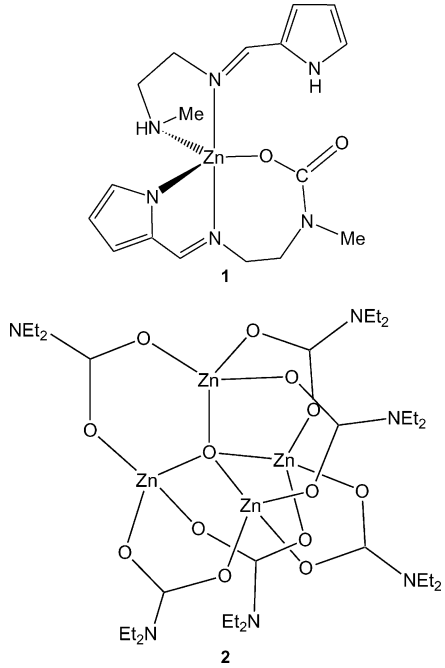

Scheme 1.

[a] Anorganisch-Chemisches Institut, Ruprecht-Karls-Universität Heidelberg,
Im Neuenheimer Feld 270, 69120 Heidelberg, Germany
E-mail: hans-jorg.himmel@aci.uni-heidelberg.de
Fax: +49-6221-54-5707
[b] Institut für Technische Chemie – Chemisch-Physikalische Verfahren (ITC-CPV), Forschungszentrum Karlsruhe,
Postfach 3640, 76021 Karlsruhe
Supporting information for this article is available on the WWW under http://www.eurjic.org or from the author.

to a mixture of dialkylzinc and the secondary amine (in a twofold excess) into which CO_2 had been introduced.[5,6] $[Zn_4O(O_2CNMe_2)_6]$ has been prepared (also by standard Schlenk techniques) by reaction between ZnO in acetonitrile and $[NH_2Me_2][O_2CNMe_2]$ under CO_2,[7,8] and $[Zn_4O(O_2CNBu_2)_6]$ by reaction between $ZnSO_4$, $[NH_2Bu_2][O_2CNBu_2]$ and H_2O.[9] The third route leads to complexes in which carbamato ligands replace some of the X (halogen or alkyl) ligands of ZnX_2; e.g. the tetranuclear complex $Zn_4Me_2(O_2CNEt_2)_6$[10] was isolated as product of reaction between $ZnMe_2$, $HNEt_2$ and CO_2. $Zn_4Me_2(O_2CNEt_2)_6$ has been shown to react further with $ZnMe_2$ to give $[MeZn(O_2CNEt_2)]_4$.[11] Other complexes of the general formula $[MeZn(O_2CNR_2)]_4$ (R = *i*Pr and *i*Bu) were synthesized directly from $ZnMe_2$, the corresponding secondary amine and CO_2.[12] From these examples it can already be concluded that slight modifications could lead to different products indicating that the carbamato ligands could easily be replaced by other ligands and that the complex sizes could vary.

Despite the richness of different carbamate complexes which have been isolated, surprisingly little is known about their reactivity. Four examples are as follows: (i) Complexes of the formula $[RZn(O_2CNR_2)]_4$ were treated with pyridine (py) leading to decomposition of the tetrameric complex to give dimeric complexes of the formula $[R(py)Zn(O_2CNR_2)]_2$.[12] (ii) $[OZn_4(O_2CNR_2)]_6$ complexes are amenable to transamination,[5] leading effectively to an exchange of the R groups. (iii) The CO_2 units in $[OZn_4(O_2CNR_2)_6]$ complexes can also be replaced, as shown by experiments with ^{13}C-enriched CO_2;[6] this reaction shows that the bonding situation in these carbamate complexes is reminiscent of the bonding situation in enzymes featuring carbamate units and also in other transition metal carbamate complexes. (iv) As already mentioned, $[Zn_4Me_2(O_2CNEt_2)_6]$ has been shown to react with $ZnMe_2$ to give $[MeZn(O_2CNEt_2)]_4$[11] and with TMEDA (tetramethylethylenediamine) to give the mononuclear bis(carbamate) complex $[(Et_2NCO_2)_2Zn(TMEDA)]$.[13]

Herein we report on the synthesis and characterisation of some new zinc carbamates which were synthesised in high yields according to the third route in Scheme 2. In addition to the experiments, quantum chemical calculations were carried out, the results of which have shed further light on some of the structures and reactions. These calculations build upon the detailed analysis of possible mechanisms published previously.[14] Furthermore, we analysed the decomposition of the carbamate complexes. Applying various techniques, we show that the complexes decompose below 200 °C to give ZnO nanoparticles which might find application in catalysis or for optoelectronic devices. An analysis of the powder diffraction data and BET and TEM measurements show that all ZnO particles have about the same size of ca. 10 nm. The decomposition temperature is similar to that observed for $[MeZnOR]_4$ (R = *t*Bu or *i*Pr) complexes which have been recently shown to be valuable precursors to catalytically active ZnO.[15] In addition to its catalytic properties, ZnO can be used for a variety of applications including optoelectronics in the blue and ultraviolet (UV) spectroscopic region (e.g. light-emitting diodes, laser diodes and UV detectors) and as gas sensors, surface acoustic wave devices, varistors, piezoelectric transductors or window material for displays and solar cells.[16]

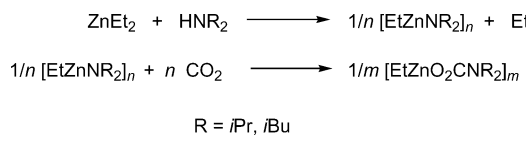

Scheme 2.

Results and Discussion

A toluene solution containing equimolar quantities of diethylzinc and the secondary amine $HN(iPr)_2$ was stirred at 70 °C for 3 h. The NMR spectrum recorded after this period turned out to be basically a superposition of the signals of the starting reagents $ZnEt_2$ and $HN(iPr)_2$. On the other hand, after stirring at room temperature for 3 d, the spectra indicated almost quantitative formation of $EtZnN(iPr)_2$ (**3**; see Supporting Information). Previous reports show that zincation of amines in toluene is a relatively slow reaction.[17] For example, $MeZnN(H)Si(iPr)_3$ has been synthesised by stirring $H_2NSi(iPr)_3$ together with $ZnMe_2$ in toluene at room temperature for 10 h and subsequently under reflux for an additional 2 h.[18] Without isolation of the amide **3**, CO_2 was passed at room temperature through the reaction mixtures for 30 min. Surprisingly, the resultant carbamate product (vide infra) proved to be identical, irrespective of the time and temperature at which the $ZnEt_2$/$HN(iPr)_2$ mixture had been stirred. Similar reactions were carried out with $HN(iBu)_2$. Fixation of CO_2 in this case was also possible not only after formation of $EtZnN(iBu)_2$ (**4**) was completed, but straight away from the $ZnEt_2$/$HN(iBu)_2$ reaction mixture. Most likely, CO_2 attacks the amine, and the resultant species (adduct in equilibrium with the unstable carbamic acid) reacts much faster with $ZnEt_2$ than does the amine. We did not attempt to isolate the alkylzinc amide, since crystal structures for related compounds such as $[EtZnNHSi(iPr)_3]_2$[18] are already known and reveal the presence of dimeric units. In solution, dimers and monomers should exist in equilibrium (vide infra). Quantum chemical calculations [BP/SV(P)] were carried out to analyse the monomer/dimer equilibrium of **3** with some parameters calculated for monomeric and dimeric **3** being summarised in Table 1 (see also Supporting Information). The calculations suggest a dimerisation energy for **3** (see Scheme 3) of –88 without and –79 kJ mol^{-1} including ZPE corrections. ΔG^0 (at 1 bar, 298 K) for the (gas-phase) reaction was calculated to be not more than –2 kJ mol^{-1}. Therefore, one expects an equilibrium for **3**. Since the solvent used in the experiments is toluene, necessary corrections due to the solvent effect are very small (probably of the same order as the error caused by the approximations implied in models such as COSMO).[14] Quantum chemical calculations on

the NMR shifts show that the monomer and the dimer exhibit only slightly different chemical shifts (see Supporting Information) making it difficult to distinguish between them. Thus, according to the calculations, the C atom directly attached to the Zn atom should give rise to a signal in the ^{13}C NMR spectra at δ = 8.0, 7.5 and 8.1 ppm for $ZnEt_2$, monomeric and dimeric **3**, respectively (referenced to tetramethylsilane). The experimental ^{13}C NMR spectra in C_6D_6 show corresponding signals at δ = 0.17 and 6.27 ppm for $ZnEt_2$ and **3**, respectively.

Table 1. Some parameters (bond lengths [pm], bond angles [°]) calculated [BP/SV(P)] for monomeric and dimeric **3** and **4**.

	3		**4**	
	Monomer	Dimer	Monomer	Dimer
Zn–N	185.1	209.3–211.1	185.2	207.4–210.2
Zn–C	195.3	199.9/200.2	195.2	199.6/199.8
N–C	145.7/146.2	148.8–149.6	145.2	147.0–148.6
C–C–Zn	115.8	116.9/117.2	116.0	116.2/116.7
C–Zn–N	178.2	128.6–138.5	174.1	133.6–136.0
Zn–N–Zn		86.5		88.7/89.2
N–Zn–N		92.7/92.9		90.2/90.6

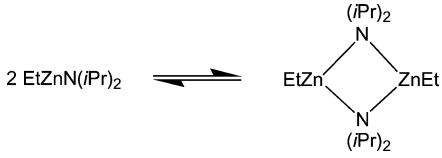

Scheme 3.

Dimeric and monomeric species should also be in equilibrium in the case of solutions containing **4**. Quantum chemical calculations carried out for the monomer indicated an interesting structural detail (see Figure 1). Thus, a CH···Zn contact is established exhibiting an H···Zn distance of 233.3 pm according to BP86/SV(P) data. Additional calculations at the B3LYP/TZVPP level of theory also resulted in a similar minimum structure in which the CH···Zn contact is longer (244.4 pm) but still present (see Supporting Information for a list of all coordinates). In the case of **4**, dimerisation is associated with an energy change of –78 without and –71 kJ mol^{-1} with ZPE corrections, and ΔG^0 amounts to –4 kJ mol^{-1}. As anticipated, these values are close to those calculated for **3**. The position of the monomer/dimer equilibrium can be shifted to the monomer side by use of a chelating base such as TMEDA.[14] However, in these TMEDA-stabilised monomers the zinc atom is already fourfold coordinated so that one does not necessarily expect the presence of additional C–H···Zn contacts. Therefore, it will be difficult to study this possible contact experimentally.

The ^{13}C NMR spectra recorded upon CO_2 insertion very clearly showed the presence of carbamate units. Thus, signals at δ = 163.04 and 164.69 ppm can be assigned to the central C atom of the carbamato ligands in **5** ($[EtZn\{O_2CN(iPr)_2\}]_4$) and **6** ($[EtZn\{O_2CN(iBu)_2\}]_4$), respectively. Colourless crystals of the two carbamate complexes, obtained in good yields, were grown from these solutions. Compound **5** crystallises in the tetragonal space group $P4(1)$ and **6** crystallises in the triclinic space group $P\bar{1}$. In Figures 2 and 3 the structures, as determined by X-ray diffraction, are illustrated, and Tables 2 and 3 summarise some salient parameters. According to our X-ray diffraction experiments, both molecules feature two Zn_2O_3C rings which are linked by bridging O atoms. Thus, as anticipated, the structures are similar to those reported for $[MeZn\{O_2CN(iPr)_2\}]_4$ and $[MeZn\{O_2CN(iBu)_2\}]_4$.[12] The centre of inversion as the only symmetry element for crystals of **6** is clearly visible in Figure 4, showing a section of the 3D arrangement of molecules hosting the *b*- and *c*-axes

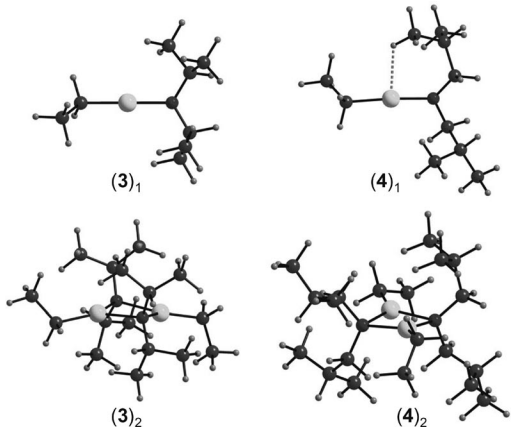

Figure 1. Structures calculated for monomeric and dimeric $EtZnN(iPr)_2$ (**3**) and $EtZnN(iBu)_2$ (**4**).

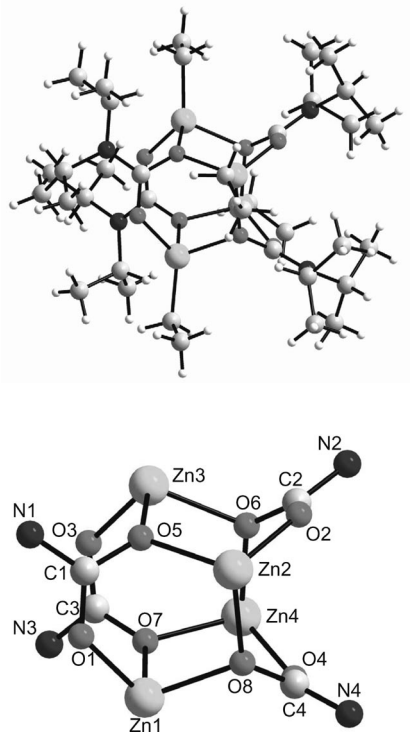

Figure 2. Structure of $[EtZn\{O_2CN(iPr)_2\}]_4$ (**5**) in the crystalline phase as determined by X-ray diffraction.

of the unit cell [a = 12.8820(16) Å, b = 13.4530(27) Å, c = 18.0890(36) Å] in the paper plane. The crystal structure of $[MeZn\{O_2CN(iBu)_2\}]_4$ was shown to be of much higher symmetry (see the comparison in Table 4).[12] In agreement with the work in ref.[12], the formation of $[Et_2Zn_4\{O_2CN(iPr)_2\}_6]$ or $[Et_2Zn_4\{O_2CN(iBu)_2\}_6]$ as reported in ref.[10] for a closely related reaction was not observed.

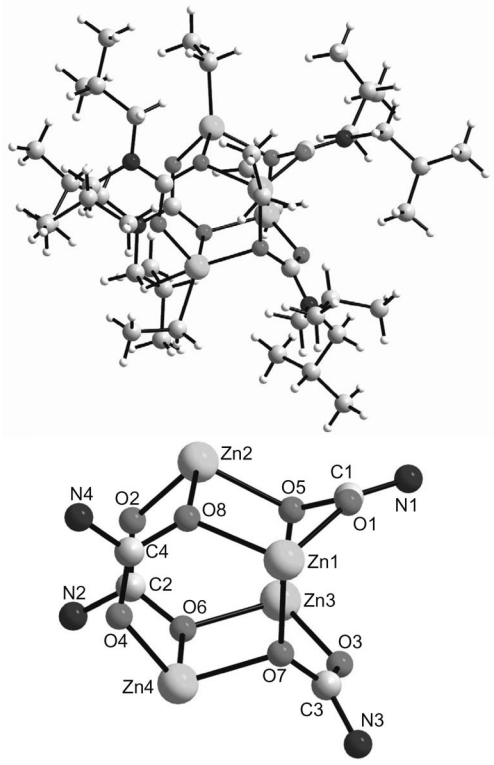

Figure 3. Structure of $[EtZn\{O_2CN(iBu)_2\}]_4$ (**6**) in the crystalline phase as determined by X-ray diffraction.

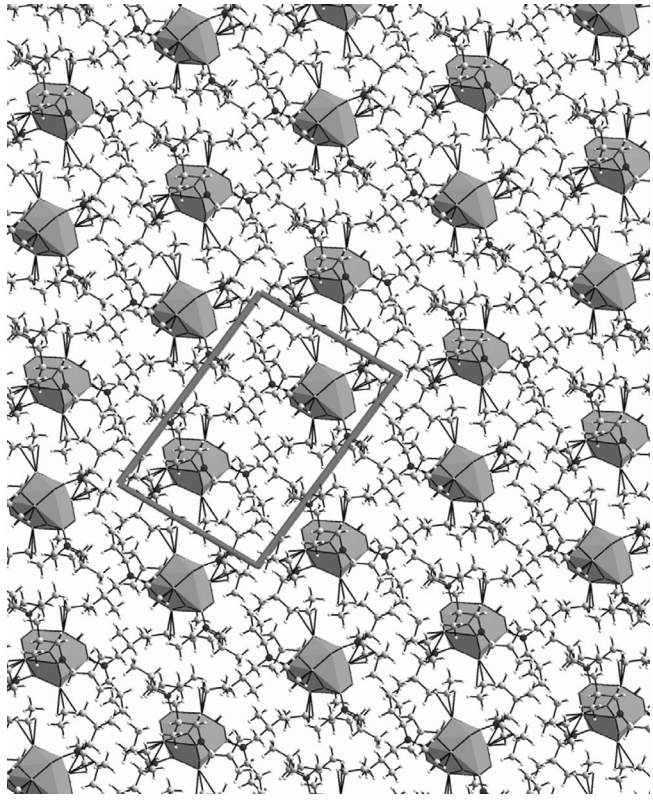

Figure 4. Arrangement of molecules of **6** in the crystalline phase as determined by X-ray diffraction.

Table 2. Selected bond lengths [pm] and angles [°] for **5** as determined by X-ray diffraction.

Zn1–C	196.6(4)	Zn2–C	1.968(4)
Zn1–O1	196.6(4)	Zn2–O2	196.5(3)
Zn1–O7	206.2(3)	Zn2–O5	209.9(2)
Zn1–O8	208.8(3)	Zn2–O8	207.4(3)
Zn3–C	195.8(5)	Zn4–C	196.2(4)
Zn3–O3	198.5(3)	Zn4–O4	195.0(3)
Zn3–O5	204.8(3)	Zn4–O6	207.1(2)
Zn3–O6	206.6(2)	Zn4–O7	205.8(3)
O1–C1	125.6(4)	O5–C1	130.5(4)
O2–C2	125.9(4)	O6–C2	130.6(4)
O3–C3	127.4(6)	O7–C3	130.1(5)
O4–C4	127.2(5)	O8–C4	130.1(4)
N1–C1	134.4(5)	N3–C3	133.0(5)
N2–C2	134.9(5)	N4–C4	133.1(5)
C–Zn1–O1	124.29(17)	C–Zn3–O3	118.2(2)
C–Zn1–O7	120.58(19)	C–Zn3–O5	125.29(17)
C–Zn1–O8	112.79(19)	C–Zn3–O6	112.39(19)
O1–Zn1–O7	97.28(11)	O3–Zn3–O5	100.99(12)
O1–Zn1–O8	102.41(11)	O3–Zn3–O6	102.80(12)
O7–Zn1–O8	94.14(10)	O5–Zn3–O6	92.42(10)
C–Zn2–O2	129.11(17)	C–Zn4–O4	124.51(16)
C–Zn2–O5	108.89(18)	C–Zn4–O6	118.28(17)
C–Zn2–O8	119.19(15)	C–Zn4–O7	118.85(16)
O2–Zn2–O5	98.75(11)	O4–Zn4–O6	100.22(13)
O2–Zn2–O8	98.43(12)	O4–Zn4–O7	95.94(13)
O5–Zn2–O8	96.26(10)	O6–Zn4–O7	92.47(10)

Table 3. Selected bond lengths [pm] and angles [°] for **6** as determined by X-ray diffraction.

Zn1–C	198.3(4)	Zn2–C	196.4(5)
Zn1–O1	195.6(3)	Zn2–O2	199.4(3)
Zn1–O7	210.2(3)	Zn2–O5	206.2(3)
Zn1–O8	209.6(3)	Zn2–O8	210.6(3)
Zn3–C	197.2(4)	Zn4–C	197.4(4)
Zn3–O3	197.9(3)	Zn4–O4	197.1(3)
Zn3–O5	208.1(3)	Zn4–O6	206.6(3)
Zn3–O6	207.0(3)	Zn4–O7	206.9(3)
O1–C1	125.5(5)	O5–C1	130.9(5)
O2–C2	126.8(5)	O6–C2	130.5(5)
O3–C3	126.9(5)	O7–C3	131.0(5)
O4–C4	125.6(5)	O8–C4	130.1(5)
N1–C1	133.3(5)	N3–C3	133.8(5)
N2–C2	134.1(5)	N4–C4	134.3(5)
C–Zn1–O1	123.73(17)	C–Zn3–O3	127.35(15)
C–Zn1–O7	116.43(16)	C–Zn3–O5	116.96(15)
C–Zn1–O8	116.18(16)	C–Zn3–O6	116.80(16)
O1–Zn1–O7	100.47(11)	O3–Zn3–O5	97.19(12)
O1–Zn1–O8	98.83(13)	O3–Zn3–O6	97.27(12)
O7–Zn1–O8	96.45(11)	O5–Zn3–O6	94.85(10)
C–Zn2–O2	122.02(18)	C–Zn4–O4	112.79(16)
C–Zn2–O5	118.96(19)	C–Zn4–O6	126.29(17)
C–Zn2–O8	118.97(17)	C–Zn4–O7	120.33(18)
O2–Zn2–O5	97.52(11)	O4–Zn4–O6	98.53(13)
O2–Zn2–O8	97.94(12)	O4–Zn4–O7	102.90(12)
O5–Zn2–O8	96.04(11)	O6–Zn4–O7	91.40(11)

Table 4. Crystal symmetries for the four carbamate complexes $[MeZn\{O_2CN(iPr)_2\}]_4$, $[EtZn\{O_2CN(iPr)_2\}]_4$, $[MeZn\{O_2CN(iBu)_2\}]_4$ and $[EtZn\{O_2CN(iBu)_2\}]_4$. The structural data for $[MeZn\{O_2CN(iPr)_2\}]_4$ and $[MeZn\{O_2CN(iBu)_2\}]_4$ were taken from ref.[12]

Complex	Crystal system	Point group	Unit-cell volume [Å^3]
$[MeZn(O_2CN(iPr)_2)]_4$	tetragonal	$P4(1)$	4510.3
$[EtZn(O_2CN(iPr)_2)]_4$	tetragonal	$P4(1)$	4745.3
$[MeZn(O_2CN(iBu)_2)]_4$	tetragonal	$I4$	2655.9
$[EtZn(O_2CN(iBu)_2)]_4$	triclinic	$P\bar{1}$	2815.5

Quantum chemical calculations predict the (solvent-free) reaction of CO_2 with monomeric **3** giving the tetrameric carbamate product **5** as exothermic, in agreement with the experimental results. Using BP86/SV(P), we obtained reaction energies with and without ZPE corrections of –191 and –175 kJ mol^{-1}, respectively, and a ΔG^0 value of –82 kJ mol^{-1}. The reaction proceeds rapidly at room temperature so that the activation energy is likely to be relatively low. Indeed, previous quantum chemical calculations by us confirmed that the reaction starting from the monomeric amides proceeds with virtually no activation energy.[14]

If small amounts of water are added to the reaction mixture, the carbamate complex $[OZn_4\{O_2CN(iBu)_2\}_6]$ (**7**) is formed instead of **6**. Figure 5 shows a LIFDI (Liquid Injection FD Ionisation) spectrum of **7** together with a simulation of the isotopic structure indicating that the molecule is stable in solution. In addition to the signal centred at m/z = 1310.5 resulting from $[OZn_4\{O_2CN(iBu)_2\}_6]$, a small signal centred at m/z = 1418.5 was found. Compound **7** crystallises in the orthorhombic space group *Fdd*2. A molecular C_2 rotational axis runs through atoms N1–C1–C2–N2 (see Figure 6). The central OZn_4 unit resembles the structure of solid ZnO in which Zn^{2+} cations occupy alternative tetrahedral holes in an hexagonally close-packed array of O^{2-}. The O1–Zn bond lengths of ca. 194 pm (see Table 5 for other parameters) are very close to the Zn–O distances in solid (wurtzite) ZnO (193 pm).[19] In the case of $[OZn_4(acetate)_6]$,[20] absorption and emission spectra have been measured, and they also confirm the analogy with the electronic properties of ZnO.

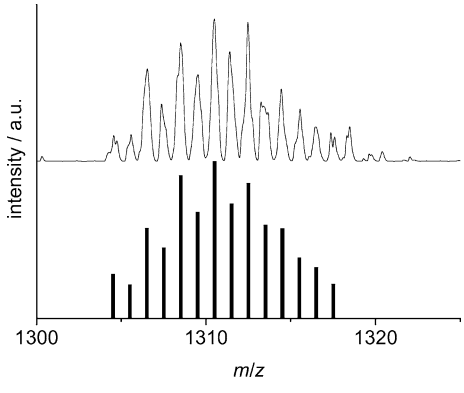

Figure 5. LIFDI spectrum of **7** in solution [measured spectrum (top) together with a simulation of the most intense isotopic peaks].

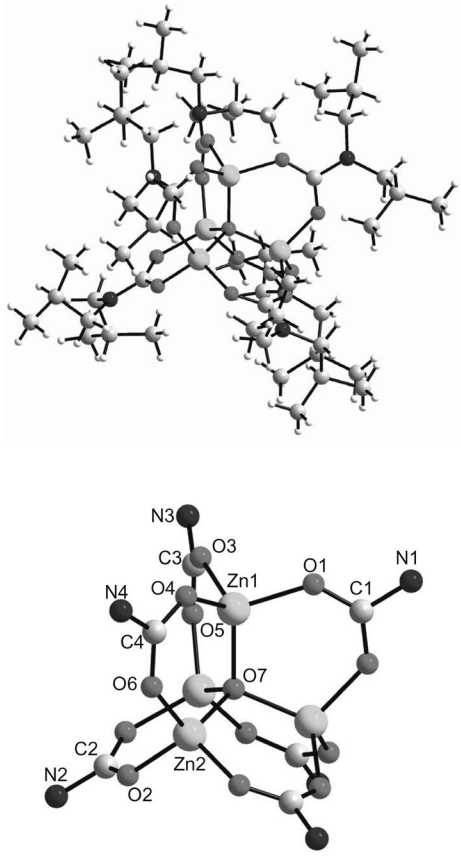

Figure 6. Structure of $[OZn_4\{O_2CN(iBu)_2\}_6]$ (**7**) in the crystalline phase as determined by X-ray diffraction.

Table 5. Selected bond lengths [pm] and angles [°] for **7** as determined by X-ray diffraction.

Zn1–O7	193.6(2)	Zn2–O7	194.6(2)
Zn1–O1	194.2(2)	Zn2–O2	194.5(2)
Zn1–O3	193.6(2)	Zn2–O5	193.4(2)
Zn1–O4	192.7(2)	Zn2–O6	192.2(2)
O1–C1	126.8(3)	O4–C4	127.5(4)
O2–C2	126.6(3)	O5–C3	127.2(4)
O3–C3	127.3(4)	O6–C4	128.1(4)
N1–C1	136.4(5)	N3–C3	134.9(4)
N2–C2	136.1(6)	N4–C4	134.2(4)
O7–Zn1–O1	108.89(10)	O7–Zn2–O2	108.58(10)
O7–Zn1–O3	111.15(8)	O7–Zn2–O5	112.21(8)
O7–Zn1–O4	113.39(8)	O7–Zn2–O6	112.48(7)
O1–Zn1–O3	107.38(10)	O2–Zn2–O5	113.54(10)
O1–Zn1–O4	111.78(10)	O2–Zn2–O6	105.94(10)
O3–Zn1–O4	104.04(11)	O5–Zn2–O6	103.93(11)
Zn1–O7–Zn1′	113.15(14)	O1–C1–O1′	125.7(4)
Zn1–O7–Zn2	108.143(14)	O2–C2–O2′	125.7(4)
Zn1′–O7–Zn2	107.558(14)	O3–C3–O5	124.9(3)
Zn2–O7–Zn2′	112.37(14)	O4–C4–O6	124.5(3)
Zn1–O7–Zn2′	107.563(14)		
Zn1′–O7–Zn2′	108.145(14)		

Thermal Decomposition

Compounds **5** and **6** decompose at relatively low temperatures. Figure 7a shows thermogravimetric (TG) curves recorded for **5** at different heating rates (2, 5 and 10 °C min^{-1}). It can be seen that the heating rate affects the

decomposition. Thus, decomposition is completed at higher temperatures for faster heating rates, arguing for a nonequilibrium process under these conditions. In Figure 7b the first derivative of the TG curve for a heating rate of 2 °C min^{-1} is shown. Two minima are visible at ca. 130 and 192 °C. Thus, as shown previously for $[RZnOR']_4$ precursor compounds [e.g. R = CH_3, R′ = $CH(CH_3)_2$], decomposition occurs in two steps.[15b] The mass loss of the two combined steps is ca. 67% which is consistent with a decomposition to give ZnO. Raman spectra were recorded before and after decomposition to obtain further information. Figure 8 displays the Raman signal of **5** in the region around 450 cm^{-1}. An additionally measured wurtzite ZnO reference (trace c) shows the characteristic two intense (allowed) E_2 phonon modes of ZnO at 98 and 437 cm^{-1} (E_2^{low} and E_2^{high}, literature values 99 and 439 cm^{-1}[21]). Other signals at ca. 330, 380 and 580 cm^{-1} were previously assigned to $E_2^{high} - E_2^{low}$, A_1(TO) and E_1(LO) (TO and LO should denote the transverse and longitudinal components, in which the infrared-active optical phonon mode is split).[22] Finally, a broad signal around 1140 cm^{-1} (see Supporting Information) is due to $2E_1$(LO), gaining intensity due to the presence of a resonance Raman effect.[23] All these signals are absent in the spectrum recorded for **5** prior to heating (trace a). The appearance of the signals characteristic for ZnO in the spectrum recorded after heating the sample to 300 °C (trace b) confirms that decomposition of **5** leads to ZnO. Importantly, the spectra show no sign of any signals besides those due to ZnO (see also the Raman spectra presented in the Supporting Information). Therefore, decomposition appears to be a clean process and the use of the carbamate complexes as ZnO precursors is attractive.

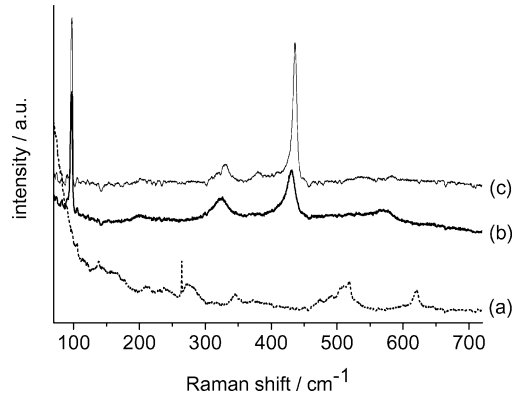

Figure 8. Raman spectra in the region around 450 cm^{-1} (excited with the 514 nm line of an Ar^+ ion laser) measured for **5** (a) before heating and (b) after heating to 300 °C, together with (c) a reference Raman spectrum of a purchased ZnO sample.

We also measured X-ray powder diffraction (XRD) data in reflection with Cu radiation. The ZnO can be identified from the powder diffractogram as the hexagonal in the space group $P6_3mc$ ($a = b$ = 324.98 pm, c = 520.66 pm, see Figure 9). The mean particle size calculated using the Debye–Scherrer equation from the line broadening in the diffractogram was 10.3 nm. This value is in good to excellent agreement with the results for the particle size determination of 10.4 nm obtained from BET measurements (BET surface: 102.7 m^2 g^{-1}, density of ZnO: 5.6 g cm^{-3}, see Supporting Information). Furthermore, these results are confirmed[24] by a statistical evaluation from the TEM measurements giving a mean particle size of 9.3(1.6) nm with a maximum in the particle size distribution at about 9.5 nm (see Figure 10). In the high-resolution TEM measurement,

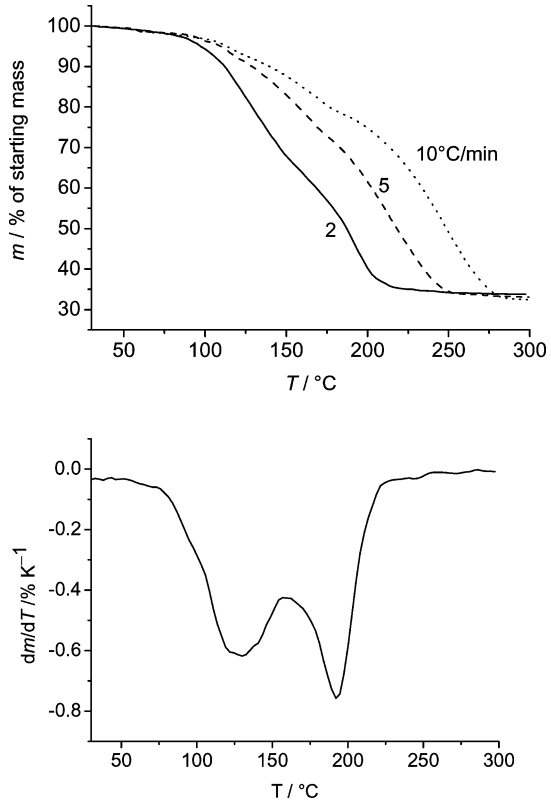

Figure 7. (a, top) Thermogravimetric (TG) curves obtained for **5** with different heating rates (2, 5 and 10 °C min^{-1}). (b, bottom) First derivative of the TG curve recorded for a heating rate of 2 °C min^{-1}.

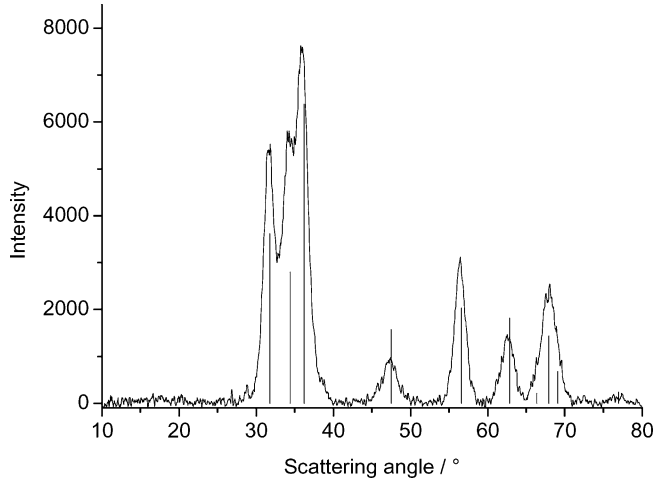

Figure 9. Powder diffraction patterns as measured after heating of **5** to 300 °C with a heating rate of 5 K min^{-1}. The inserted lines are taken from the database for ZnO.

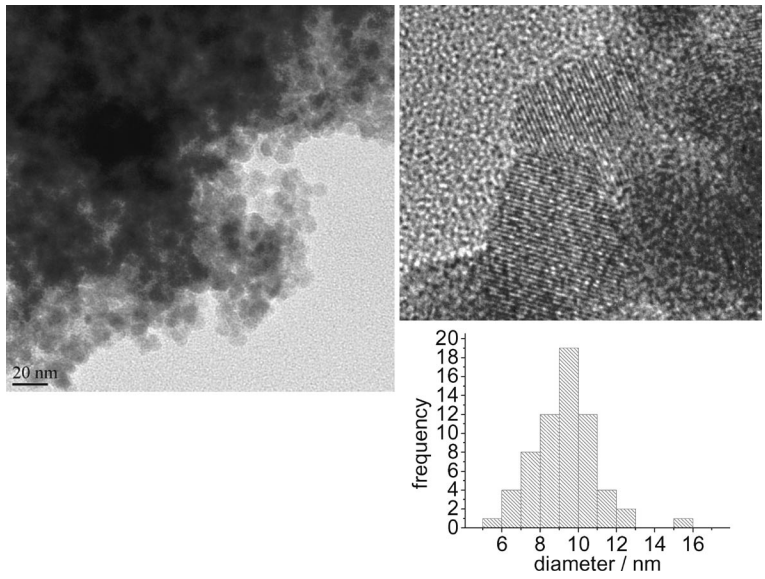

Figure 10. TEM image showing the ZnO nanoparticles formed by heating of **5** to 300 °C (heating rate 5 K min^{-1}) and plot of the size distribution.

the crystalline nature of the material is, in addition to the XRD measurements, substantiated by the existence of crystal planes in the particles. The layers of the [1,0,0] (or [0,1,0]) plane of ZnO with a corresponding plane-to-plane distance of 293(8) pm are resolved (expected 281 pm). An EDX analysis of the ZnO particles shows the presence of ca. 3% of carbon impurities which might be due to adsorbed solvent molecules. Solvent adsorption is found regularly for ZnO formation in polyol solvents.[25] All these results show that during the pyrolysis of **5**, nanoparticles of definite shape and overall good particle size distribution are formed. This gives evidence that the pyrolysis proceeding at a low temperature of 200 °C is finally a controlled process or else not so well defined particles in terms of size and crystalline behaviour would be expected as the product.

Conclusions

Reaction of diethylzinc with HN(*i*Pr)$_2$ and HN(*i*Bu)$_2$ afforded the alkylzinc amide species [EtZnNR$_2$]$_n$ (R = *i*Pr or *i*Bu). Insertion of CO_2 at room temperature into the metal–amide bond afforded the tetrameric carbamate complexes [EtZn{O_2CN(*i*Pr)$_2$}]$_4$ and [EtZn{O_2CN(*i*Bu)$_2$}]$_4$. Addition of small quantities of water results in formation of [OZn_4-(O_2CNR_2)$_6$] complexes, whereas larger amounts of water cause further decomposition and precipitation of ZnO. The new carbamate complexes were structurally characterised by X-ray diffraction. The experimental results were supplemented by quantum chemical calculations which shed light on the thermodynamics of some of these reactions. Interestingly, the carbamates thermally decompose to give ZnO nanoparticles. The decomposition process was analysed by using thermogravimetric, Raman, X-ray powder diffraction, BET, EDX and TEM measurements which show that the process is quantitative and occurs under mild conditions (below 200 °C) leading to ZnO nanoparticles with an average size of about 10 nm and a narrow size distribution. The oxygen atoms in the ZnO particles originate from the CO_2 reactant.

Experimental Section

General: All reactions were carried out under dry argon using standard Schlenk techniques. All solvents were dried by using standard methods followed by distillation. Diethylzinc as a 1.5 M solution in toluene, HN(*i*Pr)$_2$ and HN(*i*Bu)$_2$ as well as carbon dioxide were purchased from Aldrich and Acros and used as delivered. Raman spectra were recorded (without using a polarisor) with a Horiba JobinYvon Triple T64000 spectrometer equipped with a triple monochromator system and a CCD camera detector. The 514 nm line of an Ar^+ ion laser (500 mW) was used for excitation. Thermogravimetric (TG) measurements were carried out with a Mettler TC15 instrument under Ar over a temperature range of 30–600 °C. The heating rate was varied between 2 and 10 K min^{-1}. NMR spectra were recorded at room temperature with a Bruker Avance II 400 spectrometer. The chemical shifts were referenced to tetramethylsilane (TMS). The BET measurements were carried out with a Quantachrome NOVA automated gas adsorption system. TEM experiments were performed with a FEI Tecnai F20 TEM instrument with a field emission gun at 200 kV on carbon-coated 400 mesh copper grids. The XRD measurements were performed with a Siemens D500 diffractometer by using Cu radiation and with a step size of 0.1° and an irradiation time of 2° min^{-1}. The data were evaluated with EVA (DIFFRACplus, EVA 9.0, XRD evaluation program, Bruker AXS, 2003). The calculation of the particle size was carried out by using the Debye–Scherrer equation.[26]

X-ray Crystallographic Study: Suitable crystals were taken directly out of the mother liquor, immersed in perfluorinated polyether oil and fixed on top of a glass capillary. Measurements were made with a Nonius-Kappa CCD diffractometer with a low-temperature unit using graphite-monochromated Mo-K_α radiation. The temperature was set to 200 K. The data collected were processed by

using the standard Nonius software.[27] All calculations were performed using the SHELXT-PLUS software package. Structures were solved by direct methods with the SHELXS-97 program and refined with the SHELXL-97 program.[28,29] Graphical handling of the structural data during solution and refinement was performed with XPMA.[30] Structural representations were generated by using Winray 32.[31] Atomic coordinates and anisotropic thermal parameters of non-hydrogen atoms were refined by full-matrix least-squares calculations. CCDC-665106, -665107, and -665108 contain the supplementary crystallographic data for this paper. These data can be obtained free of charge from the Cambridge Crystallographic Data Center via www.ccdc.cam.ac.uk/datarequest/cif.

EtZnN(*i*Pr)$_2$ (3): Diethylzinc (20 mL, 30 mmol) was treated with 1 equiv. of HN(*i*Pr)$_2$ (3.03 g, 30 mmol) in toluene (50 mL) over the weekend at room temperature under argon. The solvent was evaporated completely leaving a colourless liquid. ^{1}H NMR (400 MHz, C_6D_6): δ = 0.33 (q, ^3J = 8.16 Hz, 2 H, CH_3CH_2Zn), 1.42 (t, ^3J = 8.15 Hz, 3 H, CH_3CH_2Zn), 0.92 (d, ^3J = 6.27 Hz, 12 H, Me_2CH), 2.76 (m, ^3J = 6.31 Hz, 2 H, $CHMe_2$) ppm. ^{13}C NMR (100.56 MHz, C_6D_6): δ = 6.27 (CH_3CH_2Zn), 11.97 (CH_3CH_2Zn), 22.99 (Me_2CH), 45.65 ($CHMe_2$) ppm.

[EtZn{O$_2$CN(*i*Pr)$_2$}]$_4$ (5): Diethylzinc (20 mL, 30 mmol) was treated with 1 equiv. of diisopropylamine (3.03 g, 30 mmol) in toluene (50 mL) at 70 °C under argon for 3 h. The resultant solution was cooled to room temperature and dry CO_2 gas bubbled through for 30 min. The solvent was removed in vacuo and the solid product recrystallised from toluene/hexane (6:1) at –20 °C to give colorless cubic crystals (5.91 g, 82%). ^{1}H NMR (400 MHz, C_6D_6): δ = 0.66 (q, ^3J = 8.17 Hz, 2 H, CH_3CH_2Zn), 1.69 (t, ^3J = 8.12 Hz, 3 H, CH_3CH_2Zn), 1.13 (d, ^3J = 6.8 Hz, 12 H, Me_2CH), 3.88 (m, ^3J = 6.4 Hz, 2 H, $CHMe_2$) ppm. ^{13}C NMR (100.56 MHz, C_6D_6): δ = –2.14 (CH_3CH_2Zn), 13.36 (CH_3CH_2Zn), 20.76 (Me_2CH), 46.08 ($CHMe_2$), 163.04 (CO_2) ppm.

[EtZn{O$_2$CN(*i*Bu)$_2$}]$_4$ (6): Diethylzinc (20 mL, 30 mmol) was treated with 1 equiv. of diisobutylamine (3.87 g, 30 mmol) in toluene (50 mL) at 70 °C under argon for 3 h. The resultant solution was cooled to room temperature and dry CO_2 gas bubbled through for 30 min. The solution was then concentrated to dryness and the solid product recrystallised from hexane at –20 °C to give colourless cubic crystals (6.31 g, 79%). ^{1}H NMR (200 MHz, C_6D_6): δ = 0.67 (q, ^3J = 7.08 Hz, 2 H, CH_3CH_2Zn), 1.71 (t, ^3J = 7.18 Hz, 3 H, CH_3CH_2Zn), 0.89 (d, ^3J = 7.12 Hz, 12 H, Me_2CH), 1.99 (m, ^3J = 6.42 Hz, 2 H, Me_2CH), 3.16 (d, ^3J = 6.52 Hz, 4 H, $CHCH_2$) ppm. ^{13}C NMR (50.27 MHz, C_6D_6): δ = –0.42 (CH_3CH_2Zn), 13.10 (CH_3CH_2Zn), 20.41 (Me_2CHCH_2), 27.41 (Me_2CHCH_2), 55.91 (Me_2CHCH_2), 164.69 (CO_2) ppm.

[OZn$_4${O$_2$CN(*i*Bu)$_2$}$_6$] (7): The compound was obtained in the presence of small amounts of water in the reaction mixture. ^{1}H NMR (200 MHz, C_6D_6): δ = 0.85 (d, ^3J = 6.67 Hz, 12 H, Me_2CH), 1.97 (m, ^3J = 6.74 Hz, 2 H, Me_2CH), 3.13 (d, ^3J = 7.44 Hz, 4 H, $-CHCH_2$) ppm. ^{13}C NMR (50.27 MHz, C_6D_6): δ = 20.42 (Me_2CHCH_2), 27.63 (Me_2CHCH_2), 55.42 (Me_2CHCH_2), 164.69 (CO_2) ppm.

Quantum Chemical Calculations: Quantum chemical calculations were carried out with the aid of the TURBOMOLE program.[32] If not stated otherwise, the BP86 DFT method,[33] in combination with an SV(P) basis set,[34] was applied. A vibrational analysis was carried out for each calculated minimum. The absence of any imaginary frequency indicates that all structures converged to true energy minima. Thermodynamic properties were calculated with the freeH module as implemented in TURBOMOLE.

Supporting Information (see footnote on the first page of this article): NMR spectra for **3**, Raman spectra for **5** before and after heating to 350 °C, BET measurements on ZnO, results of the quantum chemical calculation for **3**, **4** and **5**.

Acknowledgments

The authors thank the Deutsche Forschungsgemeinschaft and the Fonds der Chemischen Industrie for their continuous financial support.

[1] J. Castro, A. Castiñeiras, M. L. Duran, J. A. Garcia-Vazquez, A. Macias, J. Romero, A. Sousa, *Z. Anorg. Allg. Chem.* **1990**, *586*, 203–208.
[2] Very recently, it has been shown that ammonium carbonate in fact is a mixture of ammonium carbamate, $[NH_4][CO_2NH_2]$, and ammonium hydrogen carbonate, $[NH_4][HCO_3]$, and does not contain any $[NH_4]_2[CO_3]$. N. Kuhn, M. Ströbele, H.-J. Meyer, *Z. Anorg. Allg. Chem.* **2007**, *633*, 653–656.
[3] J. Klunker, M. Biedermann, W. Schäfer, H. Harting, *Z. Anorg. Allg. Chem.* **1998**, *624*, 1503–1508.
[4] A. Bellfoorte, F. Calderazzo, U. Englert, J. Strähle, *Inorg. Chem.* **1991**, *30*, 3778–3781.
[5] C. S. McCowan, T. L. Groy, M. T. Caudle, *Inorg. Chem.* **2002**, *41*, 1120–1127.
[6] C. S. McCowan, M. T. Caudle, *Dalton Trans.* **2005**, 238–246.
[7] D. B. Dell'Amico, F. Calderazzo, L. Labella, F. Marchetti, *Inorg. Chim. Acta* **2003**, *350*, 661–664.
[8] D. B. Dell'Amico, F. Calderazzo, L. Labella, F. Marchetti, I. Mazzoncini, *Inorg. Chim. Acta* **2006**, *359*, 3371–3374.
[9] D. B. Dell'Amico, F. Calderazzo, S. Farnocchi, L. Labella, F. Marchetti, *Inorg. Chem. Commun.* **2002**, *5*, 848–852.
[10] M. B. Hursthouse, M. A. Malik, M. Motevalli, P. O'Brien, *J. Chem. Soc., Chem. Commun.* **1991**, 1690–1691.
[11] I. Abrahams, M. A. Malik, M. Motevalli, P. O'Brien, *J. Chem. Soc., Dalton Trans.* **1995**, 1043–1046.
[12] Y. Tang, W. S. Kassel, L. N. Zakharov, A. L. Rheingold, R. A. Kemp, *Inorg. Chem.* **2005**, *44*, 359–364.
[13] M. A. Malik, M. Motevalli, P. O'Brien, *Inorg. Chem.* **1995**, *34*, 6223–6225.
[14] H.-J. Himmel, *Eur. J. Inorg. Chem.* **2007**, 675–683.
[15] a) V. Ischenko, S. Polarz, D. Grote, V. Stavarache, K. Fink, M. Driess, *Adv. Funct. Mater.* **2005**, *15*, 1945–1954; b) S. Polarz, J. Strunk, V. Ischenko, M. W. E. van der Berg, O. Hinrichsen, M. Muhler, M. Driess, *Angew. Chem.* **2006**, *118*, 3031–3035; *Angew. Chem. Int. Ed.* **2006**, *45*, 2965–2969.
[16] For a recent work on dye-sensitised solar cells using ZnO, see: Q. F. Zhang, T. P. Chou, B. Russo, S. A. Jenekhe, G. Z. Cao, *Angew. Chem.* **2008**, *120*, 2432–2435; *Angew. Chem. Int. Ed.* **2008**, *47*, 2402–2406.
[17] Our NMR spectra are consistent with those reported previously for this amide (synthesised at 40–60 °C over 5 h in diethyl ether); see: M. A. Malik, P. O'Brien, *Polyhedron* **1997**, *16*, 3593–3599; however, they are in disagreement to an earlier work, in which the authors claim to have synthesized the amide by reaction between LiN(*i*Pr)$_2$ and EtZnCl; see: M. M. Hansen, P. A. Bartlett, C. H. Heathcock, *Organometallics* **1987**, *6*, 2069–2074.
[18] M. Westerhausen, T. Bollwein, A. Pfitzner, T. Nilges, H.-J. Deiseroth, *Inorg. Chim. Acta* **2001**, *312*, 239–244.
[19] C. H. Park, S. B. Zhang, S.-H. Wei, *Phys. Rev. B* **2002**, *66*, 73202/1–73202/3.
[20] H. Kunkely, A. Vogler, *J. Chem. Soc., Chem. Commun.* **1990**, 1204–1205.
[21] F. Decremps, J. Pellicer-Porres, A. M. Saitta, J.-C. Chervin, A. Polian, *Phys. Rev. B* **2002**, *65*, 092101-1–092101-4.

[22] C.-J. Pan, H.-C. Hsu, H.-M. Cheng, C.-Y. Wu, W.-F. Hsieh, *J. Solid State Chem.* **2007**, *180*, 1188–1192, and references given therein.
[23] J. M. Calleja, M. Cardona, *Phys. Rev. B* **1977**, *16*, 3753–3761.
[24] For a comparison of methods for particle size determination, see: A. Weibel, R. Bouchet, F. Boulc'h, P. Knauth, *Chem. Mater.* **2005**, *17*, 2378–2385.
[25] L. Poul, S. Ammar, N. Jouini, F. Fiévet, F. Villain, *Solid State Sci.* **2001**, *3*, 31–42.
[26] J. I. Langford, A. J. C. Wilson, *J. Appl. Crystallogr.* **1978**, *11*, 102–113.
[27] *DENZO-SMN, Data Processing Software*, Nonius, **1998**, http://www.nonius.com.
[28] a) G. M. Sheldrick, *SHELXS-97*, *Program for Crystal Structure Solution*, University of Göttingen, **1997**, http://shelx.uni-ac.gwdg.de/SHELX/index.html; b) G. M. Sheldrick, *SHELXL-97*, *Program for Crystal Structure Refinement*, University of Göttingen, **1997**, http://shelx.uni-ac.gwdg.de/SHELX/index.html.
[29] *International Tables for X-ray Crystallography*, Kynoch Press, Birmingham, U. K., **1974**, vol. 4.
[30] L. Zsolnai, G. Huttner, *XPMA*, University of Heidelberg, **1994**, http://www.uni-heidelberg.de/institute/fak12/AC/huttner/software/software.html.
[31] R. Soltek, *Winray 32*, University of Heidelberg, **2000**, http://www.uni-heidelberg.de/institute/fak12/AC/huttner/software/software.html.
[32] a) R. Ahlrichs, M. Bär, M. Häser, H. Horn, C. Kölmel, *Chem. Phys. Lett.* **1989**, *162*, 165–169; b) O. Treutler, R. Ahlrichs, *J. Chem. Phys.* **1995**, *102*, 346–356; c) K. Eichkorn, F. Weigend, O. Treutler, R. Ahlrichs, *Theor. Chem. Acc.* **1997**, *97*, 119–124.
[33] a) A. D. Becke, *Phys. Rev. A* **1988**, *38*, 3098–3100; b) J. P. Perdew, *Phys. Rev. B* **1986**, *33*, 8822–8824.
[34] F. Weigend, R. Ahlrichs, *Phys. Chem. Chem. Phys.* **2005**, *7*, 3297–3305.

Received: December 4, 2007
Published Online: June 3, 2008

